UC Irvine
UC Irvine Previously Published Works

Title
3D particle tracking on a two-photon microscope.

Permalink
https://escholarship.org/uc/item/0gw0j1nf

Journal
Journal of fluorescence, 16(3)

ISSN
1053-0509

Authors
Ragan, Timothy
Huang, Hayden
So, Peter
et al.

Publication Date
2006-05-01

DOI
10.1007/s10895-005-0040-1

Copyright Information

Peer reviewed

3D Particle Tracking on a Two-Photon Microscope

Timothy Ragan,[1,2,3] Hayden Huang,[1] Peter So,[1] and Enrico Gratton[2]

A 3D single-particle-tracking (SPT) system was developed based on two-photon excitation fluorescence microscopy that can track the motion of particles in three dimensions over a range of 100 μm and with a bandwidth up to 30 Hz. We have implemented two different techniques employing feedback control. The first technique scans a small volume around a particle to build up a volumetric image that is then used to determine the particle's position. The second technique scans only a single plane but utilizes optical aberrations that have been introduced into the optical system that break the axial symmetry of the point spread function and serve as an indicator of the particle's axial position. We verified the performance of the instrument by tracking particles in well-characterized models systems. We then studied the 3D viscoelastic mechanical response of 293 kidney cells using the techniques. Force was applied to the cells, by using a magnetic manipulator, onto the paramagnetic spheres attached to the cell via cellular integrin receptors. The deformation of the cytoskeleton was monitored by following the motion of nearby attached fluorescent polystyrene spheres. We showed that planar stress produces strain in all three dimensions, demonstrating that the 3D motion of the cell is required to fully model cellular mechanical responses.

KEY WORDS: Particle tracking; two-photon; cell mechanics.

INTRODUCTION

Single particle tracking (SPT) records the position of a single particle with microscopic resolution as a function of time providing information about the kinetics and dynamics of a single particle rather than the ensemble averaged behavior of a population. SPT can achieve a spatial resolution as high as 5 nm with a typical bandwidth at the video rate (33 Hz). SPT is also nondestructive allowing the biochemical microenvironment around the particle to be probed in vivo. Barak and Webb [1] developed SPT system to study the two-dimensional (2D) motion of fluorescently labeled low-density lipoprotein receptors in the plasma membrane of human fibroblasts [1]. The technique was extended by using video microscopy and small gold particles (20–40 nm) as the label for the particle of interest [2]. Other groups investigated lipid motion using a high speed video camera and obtained a frequency response of 40 kHz and a precision of 17 nm [3,4]. Kis-Petikova developed a technique to track particles in 2D using the two-photon microscope [5]. Other groups have reported very high positional accuracies with lower temporal resolution [6]. In the last decade, single particle tracking has proven itself to be a very useful tool for biological studies.

A limitation of previously mentioned SPT systems is that they are restricted to tracking particles in 2D. However, many biological systems are inherently 3D and a 2D projection of the motion in certain cases may be inadequate to describe the phenomena. By employing 4D microscopy, it is possible to track particles in all three dimensions [7–10]. However, these techniques typically suffer from poor time resolution, which arises from the necessity of having to acquire multiple wide-field images for each 3D stack. The time resolution can be improved by

[1] Department of Mechanical Engineering, Massachusetts Institute of Technology, Cambridge, Massachusetts.
[2] University of Illinois at Urbana-Champaign, LFD/Physics, 1110 West Green Street, Urbana, Illinois 61801.
[3] To whom correspondence should be addressed. E-mail: tragan@mit.edu.

using a 3D SPT system based on total internal reflection [1]. However, the axial range is limited to within 250 nm of the surface of the coverslip. Peters *et al.* developed a 3D single particle system that measured the intensity changes of spheres in the center of a focused laser beam. They used this method to follow the 3D motion of receptors in the plasma membrane [12]. Spedel developed a method using off-focus imaging to track particles at 10 Hz rate but it is limited to a few micrometers in axial extent [13]. Kao and Verkman developed 3D SPT system by employing cylindrical optics that broke the axial symmetry of the optical system [14]. In a well-corrected optical system, the image of a point source should look identical at equivalent distances above or below the focus of the objective. By purposely introducing aberrations (in this case astigmatism) this symmetry is broken and the intensity distribution of the point spread function appears different depending on whether the focus is below or above the particle. They then used the centroid of the image to recover the radial coordinates of the particle and an analysis of the intensity distribution of the point spread function to determine the *z*-position. However, the system they constructed had a limited axial range and a frequency response 3–4 Hz.

We report on two different methods for fast 3D SPT studies based on the inherent 3D localization of two-photon microscopy. The performance characteristics of this system has been quantified in well-characterized test systems, and fast 3D SPT was subsequently used to study the 3D strain developed in the cytoskeleton of 293 kidney cells subjected to a locally applied force.

EXPERIMENTAL SECTION

Materials

Bead Protocol

For the cell experiments, 0.5 μm diameter polystyrene beads from Duke Scientific (Palo Alto, CA) were used. The beads were coated with human plasma fibronectin by passive adsorption, which served as a linker to integrin receptors in the plasma membrane of the cells. The coating and preparation processes for the cells were identical to the method described previously [15].

The magnetic beads were prepared with a tosylactivation protocol for a fibronectin coating according to the manufactrer's instructions. Approximately 2–3 μL of the suspension containing the beads were added to coverslip-plated cells to attain an appropriate density of bead attachments per cell.

Cell Culture

Glass coverslips were incubated in Hanks Balanced Salt Solution with fibronectin at 2 μg/mL overnight at 4°C. Two hundred and ninety-three kidney cells from the National Institute of Health were then plated on the coverslips and 1 mL of Dulbecco's modified Eagle's medium and 10% fetal calf serum was added. The cells were then incubated overnight, and then washed the next day. The experiments on the cells were performed within the next two to three days. Approximately 30 min before the start of the experiment, 2–3 μL of the suspension of magnetic beads and 1–2 μL of the polystyrene beads were added at the same time to the cells.

Methods and Apparatus

Magnetic Trap

A single pole magnetic trap was used to apply a mechanical force to the cell. The design of the pole was similar to the poles described previously [15]. Briefly, the magnetic trap consisted of a steel pole with a tapered point constructed from CMI-C steel and wrapped 550 times with a No. 24 gauge wire. The magnetic trap was mounted on a translation stage such that the trap could be positioned within several microns of the coverslip surface. This design allows the generation of forces of the order of nanonewton (nN) to be applied to paramagnetic particles attached to the cell surface.

The magnetic field distribution generated by a single pole trap is nonuniform. The magnitude of the force delivered by the magnetic trap is proportional to the product of the magnetic field strength and the magnetic field gradient. Both the magnetic field strength and its gradient decrease rapidly away from the pole tip. The exact force exerted on a paramagnetic particle at a given current is a function of the particle distance from the pole tip, and the determination of the magnetic force dependence on distance requires calibration. An efficient method to calibrate this dependence involves observing the motion of magnetic beads suspended in a fluid of known viscosity. By tracking the position of the particle with a video camera, while a force is applied, we can calculate the force the particle experience from the Stokes equation:

$$F = 3\pi \eta R v \tag{1}$$

where η denotes the viscosity of the fluid, R the bead diameter, and v the relative velocity between fluid and bead, which is determined by numerically differentiating the bead position with respect to time. In the force calibration experiments we were able to demonstrate the ability to generate forces between 100 pN and 15 nN

on 4.5 μm diameter beads (DYNABEADS M-450, Dynal, Oslo, Norway) at a distance of 10–100 μm from the magnetic pole (see Fig. 1a). Additionally, by altering the current in the coil we could vary the force that the particle would experience as is shown in Fig. 1b.

Two-Photon Microscope

The two-photon microscope system used in this study has been described previously [15]. Briefly, the microscope system is based around a modified Zeiss 100 Axiovert Microscope (Zeiss Inc., Thornwood, NY). The excitation light is provided by a Mira 900 Titanium Sapphire laser system (Coherent, Inc., Palo Alto, CA).

Fig. 1. (a) Several calibration curves used for calculating the force applied to 4.5 μm beads as a function of distance from the magnetic trap. (b) As the current through the magnetic pole is increased, the force applied to the magnetic beads increases. This increase is not linear due to saturation effects in the paramagnetic beads.

The laser light is directed into the microscope by an X-Y-galvanomotor scanning system (Cambridge Technologies, Watertown, MA), which allows the laser light to be raster scanned across the image. The laser then enters the microscope through a modified epiluminescence light path and is reflected by a dichroic filter (Chroma Technology Brattleboro, VT) to an infinity-corrected objective lens that focuses the light onto the sample. The objective is mounted on a piezo-drive that allows the objective to be moved with respect to the sample. The generated fluorescence is collected by the same objective and passes through the dichroic filter and tube lens, and is then focused onto a Hamamatsu R7400-P photomultiplier tube operating in single-photon counting mode. The TTL output from the PMT module is sent to a custom built PCI card in a computer workstation. The PCI card counts the pulses from the PMT module and also controls the XY and piezo scanners. The acquired data is transferred to a Windows application that displays the data on the screen and implements the tracking protocol.
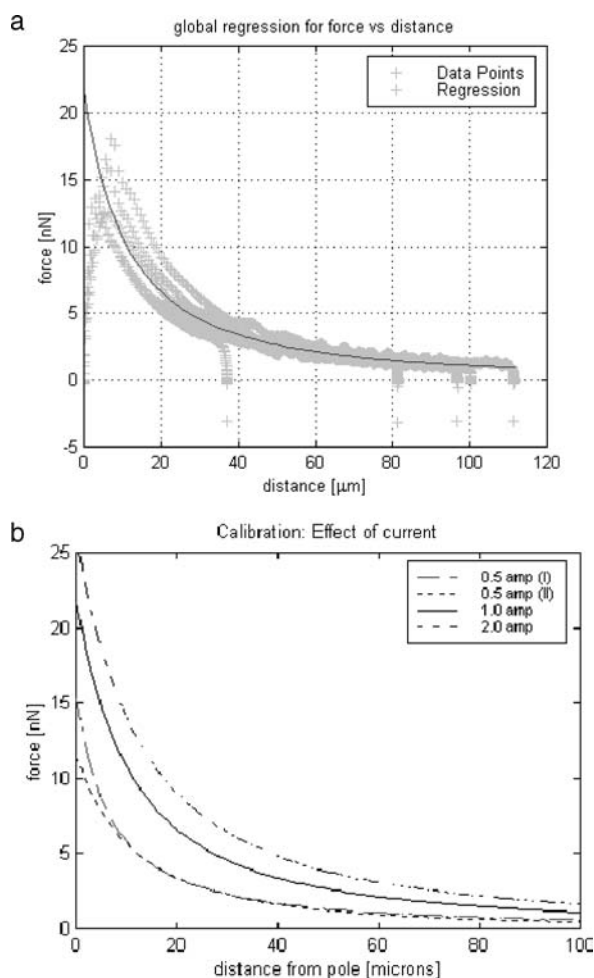
Tracking Methods

We have implemented two different techniques to accomplish 3D tracking using the two-photon microscopy. The first method is a 3D volumetric scanning that localizes the particle by scanning several images at different depths into the sample. The second technique is similar to Kao and Verkman's approach in that it utilizes aberrations in the PSF to determine the axial position of the particle [14].

There are three main ideas behind both of these techniques. The first is that the 3D resolution of two-photon microscopy assists in localizing the axial position of the particle. The second idea is that by scanning a small region in the vicinity of the particle we can achieve a higher frequency response than we could if we were imaging the whole area of the cell. The third idea is the incorporation of active feedback control in the tracking routine. By computing the instantaneous changes in the position of the particle and then quickly recentering the scan region around the particle, we can dynamically follow the motion of the particle over extended distances even though we are only scanning a small region at any given time.

A key feature of the system is that we save the images generated by the computer for further analysis. Thus, any artifacts that might occur (such as another particle diffusing into the scan area) can be detected by postexperiment inspection of the data. In addition, this allows us to apply more computationally demanding algorithms to determine the position of the particle with a higher precision. Furthermore, the cellular environment in the immediate

vicinity of the particle can be assayed based on the image morphology and fluorescent spectroscopy.

At the end of a track sequence, we have a temporal sequence of images and the coordinates of the origin of the image. To ensure the accuracy of the time separation between data points in the sequence, we stamped each image with the output of a hardware generated 33 MHz digital clock giving submillisecond accuracy. We can reconstruct the particle's full 3D trajectory from the position of the origin of the image and the information about the particle position contained in the image.

Volumetric Tracking Method

For the feedback volumetric imaging approach, a high speed piezoelectric objective driver is used to image several (typically 3–6) planes around the position of the particle. A centroid calculation is used to provide a feedback signal to reposition the scan region by offsetting the origin of the new scan, so that the particle would be in the center of the new scan region. The size of the image volume and the number of image planes in the stack are chosen to minimize the data acquisition time while maintaining a high probability, so that the particle will not diffuse beyond the cube boundary between the updates of the feedback signals. The maximum frequency response of the system is currently 3–6 Hz when operating in the volumetric tracking mode.

Aberration Tracking Method

The other method we have implemented to track particles in three dimensions involves introducing aberrations that break the axial symmetry of the PSF of the optical system of the microscope. This symmetry breaking allows us to determine the full 3D position of the particle by merely scanning a single X–Y plane in the vicinity of the particle. In a well-corrected optical system, there is little difference in the images of a point object located at equivalent distances above and below the focal plane. However, in an optical system with appropriate aberrations, axial asymmetry in the PSF can be used to determine the magnitude and direction from the focus of the objective.

An astigmatism can be introduced into an optical system by the addition of a cylindrical element; uniaxial bending of the normally flat dichroic mirror provides the required cylindrical element without adding optical elements. Figure 2a is a plot of the PSF at several axial positions and it clearly shows the aberrations. There are many methods for quantifying the aberration along the optical axis. A simple and accurate way to make this de-

termination is to calculate the generalized moment of the image

$$\text{GM} = \left(\frac{M_{yy} - M_{xx}}{M_{yy} + M_{xx}} \right) \tag{2}$$

where M_{yy} and M_{xx} are the second moments of the images:

$$M_{xx} = \frac{\sum_i x_i^2 I_i - \sum_i x_i I_i}{\sum_i I_i},$$

$$M_{yy} = \frac{\sum_i y_i^2 I_i - \sum_i y_i I_i}{\sum_i I_i} \tag{3}$$

x_i and y_i are the pixel position at the ith pixel, and I_i is the intensity at that position. The second summations in both the expressions represent the application of the parallel axis theorem and allow the evaluation of the image shape while disregarding the absolute position of the intensity distribution in the image.

Figure 2b is a plot of the GM in the region around the focus for the PSF pictured in Fig. 2a. The GM curve is most sensitive to the particle's position when the particle is very near to the focus and it serves as a sensitive measure of the axial position of the particle. The maximum frequency response of the system is currently 28 Hz. The focusing depth of the piezo stage controlling the objective limits the axial range of the system to approximately 100 μm.

EXPERIMENTAL RESULT AND DISCUSSION

Instrument Performance

To evaluate the performance of the tracking system, we performed several experiments. We tracked the position of yellow latex fluorescent spheres (Molecular Probes, Eugene, OR), dried onto a coverslip and in sucrose solution of varying concentrations. The sucrose concentration was varied to achieve a range of diffusion of coefficients. We observed both free diffusion and diffusion with flow, and the recovered diffusion coefficients from the SPT trajectories agreed well with the Stokes–Einstein relationship.

Particle Attached to the Coverslip

Two hundred-nanometer latex spheres were dried on a coverslip and mounted on an *xy*-stage. We obtained a standard deviation of approximately 30 nm in both radial directions and 40 nm in the axial direction for nonmoving particles using the aberration tracking method (Fig. 3a).
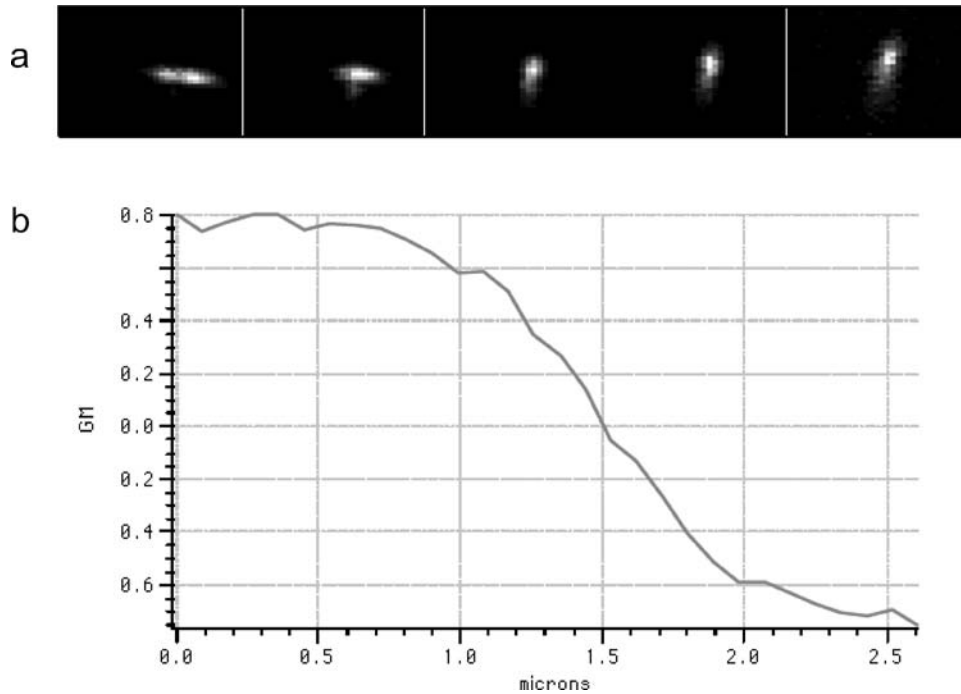
Fig. 2. (a) Images of the aberration in the point-spread function of the objective. The five images are taken at successive depths of 0.75 μm from one another. (b) The recovered generalized moment curve for a 200 nm polystyrene sphere.

This is higher than what would be expected from the photon count rate for the particles, but is consistent with what we obtained with standard wide-field video microscopy obtained on the same microscope. These noise levels were attributed to vibrations in the room as the optical table was not vibration isolated. As shown in Fig. 3b the accuracy of the instrument improves when recording the inter-particle distance between the two particles.

To move the sample in well-defined trajectories a linear variable differential transformer (LVDT) feedback controlled XY piezo-stage (P-730 Piezo XY-scanner with E-612.C0 controller) was mounted on the microscope in a vertical position such that the sample could be moved along the optical axis of the microscope system and along one of the radial axes in well-defined trajectories. The particular data sets shown in Fig. 3c and d were obtained with the aberration method and with a tracking frequency response of 14 Hz and are representative of the tests we performed using the XY piezo stage.

Free Diffusion

Next, we tracked 200 nm latex spheres in sucrose solutions. The two types of motion we expect for trajectories in solution are pure diffusion and diffusion with flow. Diffusion with flow will occur if the system contains con-

vection currents; otherwise, we will have pure diffusion. Both modes of motion are well characterized mathematically and can be summarized using mean square distance (MSD) plots

$$\text{MSD}_n = \text{MSD}_x(n\,\Delta t) + \text{MSD}_y(n\,\Delta t) + \text{MSD}_z(n\,\Delta t) \tag{4}$$

$$\text{MSD}_p(n\,\Delta t) = \frac{\sum_{i=0}^{N}(p_{i+n} - p_i)^2}{N+1} \tag{5}$$

Pure diffusion and diffusion with flow are represented mathematically by:

$$\langle r^2 \rangle = 6Dt \qquad \text{(pure diffusion)} \tag{6}$$

$$\langle r^2 \rangle = 6Dt + (Vt)^2 \qquad \text{(diffusion with flow)} \tag{7}$$

Figure 4b shows a typical trajectory of particles tracked in 60% sucrose. The motion appears to be Brownian in all three dimensions. The resulting MSD curves in Fig. 4a are very nearly straight lines which we would expect from pure Brownian motion, and the motion is roughly isotropic as evidenced by the individual slopes of the MSD plots that are approximately one-third the slope of the radial MSD. The recovered parameters from the linear fits to the short lag time MSD plots in Eq. (6) are
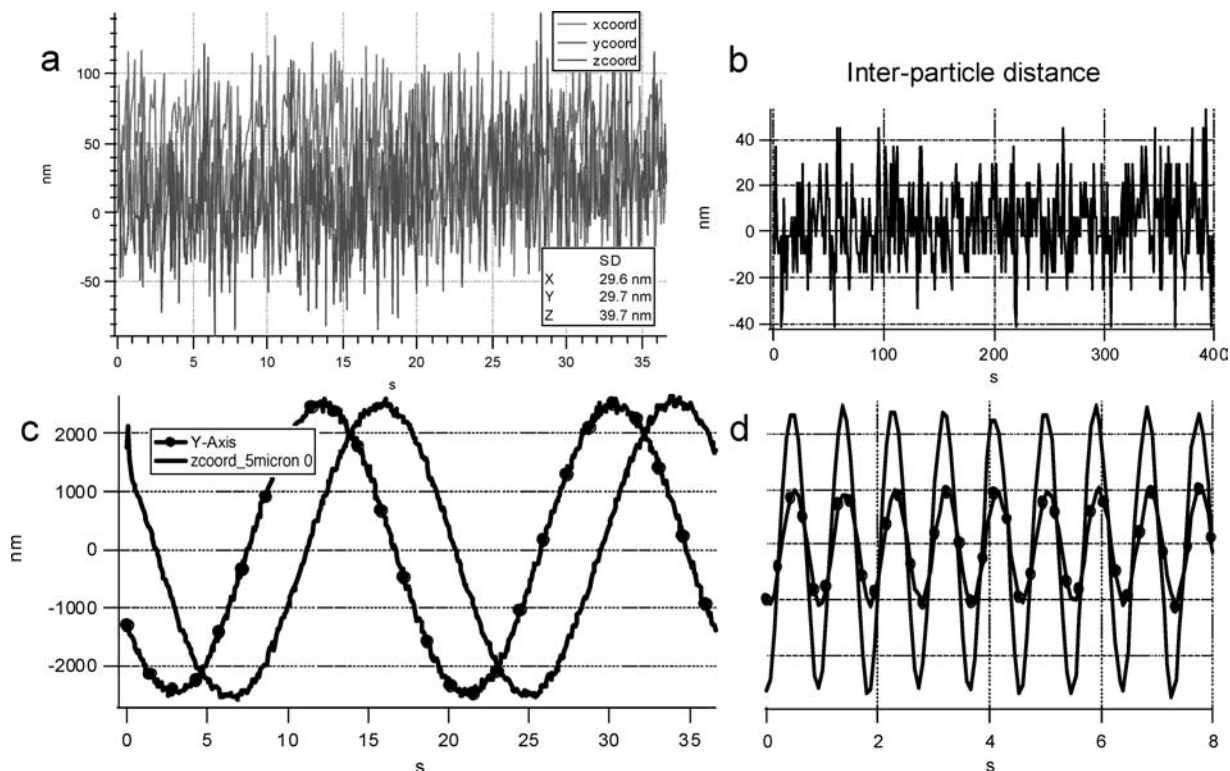
Fig. 3. Recovered trajectories obtained from tracking particles dried on a coverslip. The entire sample was mounted to an XY piezo scanner attached to the microscope stage. This way, the particle could move along both the z and y axis independently in a well-defined trajectory. (a) Nonmoving 200 nm latex sphere tracked using the aberration method. As explained in the text, the higher than expected standard deviation values are attributed to vibrations in the optical table. (b) Using the volumetric scanning approach, the inter-particle distance between two spheres on the coverslip was measured as a function of time. The standard deviation of the distance was 14.1 nm, which is much closer to the expected value. (c) A 5 μm sine wave with a frequency of 0.1 Hz was input into the piezo stage, first along the radial direction and then along the axial direction for comparison. The recovered trajectories were within 5% of the accepted axial calibration for the microscope system and had identical frequencies given the precision of the instrument. (d) We verified that the amplitude of the input scaled appropriately by changing the amplitude of the input function as the particle moved in the axial direction. Five and 2 μm signal were separately input into the piezo, and the recovered motions were within 4% of expected value.

4.13E−10, 4.33E−10, and 4.53E−10 cm²/s, for the individual x, y, and z axes, respectively and 4.30E−10 cm²/s for the overall diffusion coefficient.

Figure 4c and d shows an example of diffusion with flow. The sample consisted of 200 nm spheres in a 50% sucrose solution, which was mixed before the start of the experiment to induce flow. To calculate the velocities, we fit the trajectory to Eq. (7), with D and V as parameters. The recovered speeds for the flow were 0.35, 0.24, and 0.19 μm/s for the x, y, and z axis, respectively and 0.467 μm/s for the overall speed. Caution must be exercised in the interpretation of the velocity parameters. We assumed uniform flow over the entire length of the trajectory, which may not be a valid assumption since the velocity could have been changing in this interval. This is a general concern when trying to apply the model of pure diffusion with flow to experimental trajectories. However, the recovered velocities were consistent with the veloc-

ities that were manually observed through wide-field illumination. The recovered value of 14.4E−10 cm²/s was within 2% of the expected value as determined from the Stokes–Einstein relationship.

Figure 5a shows a rough Gaussian distribution of diffusion coefficients for 10 different trajectories of 200 nm spheres in 60% sucrose. The average recovered value was 4.1E−10 cm²/s. This is within 10% of the value of 3.8E−10 cm²/s expected by the Stokes–Einstein relationship given by

$$D = \frac{kT}{6\pi \eta R} \tag{8}$$

where k is Boltzmann's constant, T the temperature (295 K), R the radius of the particle, and η the viscosity of the solution. We estimate that the main error in the measurement was a systemic error from inaccuracy in the concentration of the sucrose solution. For high concen-
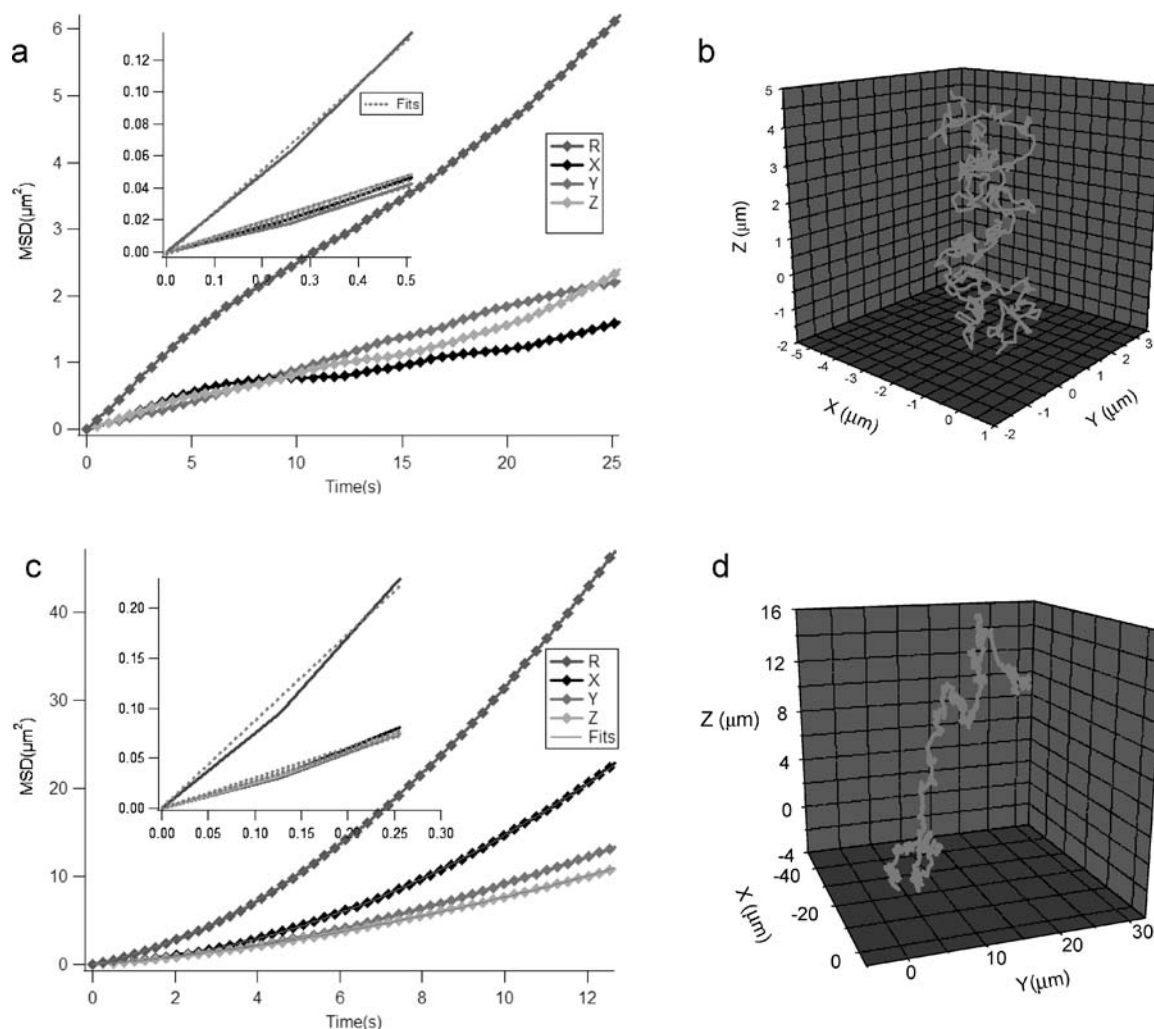
Fig. 4. (a) MSD vs. time plot for 200 nm spheres in 60% sucrose. The data consisted of a sequence of 400 coordinates that were recorded 250 ms apart with the volumetric tracking method. The inset graphs shows the MSD vs. time for short lag times up to 0.5 s, which were fit to recover the diffusion coefficient. The recovered value of 4.2E−10 cm²/s is within 10% of the expected value. (b) 3D trajectory of the sphere in 60% sucrose. (c) MSD plot of 200 nm spheres diffusing in 50% sucrose. The data consisted of 1000 coordinates that were recorded 150 ms apart and taken with the volumetric tracking method. Again, the inset graph showing MSD vs. time for short lag times was used to recover the diffusion coefficient. The recovered value of 14.4E−10 cm²/s was within 2% of the expected value as determined from the Stokes–Einstein relation. (d) 3D trajectory of the sphere in 50% sucrose with flow.

tration sucrose solutions, small errors in the concentration lead to relatively large errors in viscosity. Additional broadening of the distribution was due to imprecision arising from the heterogeneity in the size of the latex spheres that were tracked (the manufacturer quotes a standard deviation of 10 nm), and the statistical variation inherent in the stochastic nature of the calculation itself. Figure 5b is a plot of recovered diffusion coefficients for particles tracked in 60, 56, 50, and 40% sucrose. The circular data points were obtained from the aberration tracking and the square data points from the volumetric tracking method. The diffusion coefficients were plotted against inverse

viscosity. The resulting fit is linear as expected from the Stokes–Einstein relationship, and has a slope of 2.09 N, which is within 3.3% of the value of 2.16 N that we expect for the conditions of the experiment.

CELL MECHANICS

We next used this new 3D particle tracking system to study the three-dimensional response of 293 kidney cells to an externally applied force. Our study is an extension of previous work [16–20]. External force is applied via
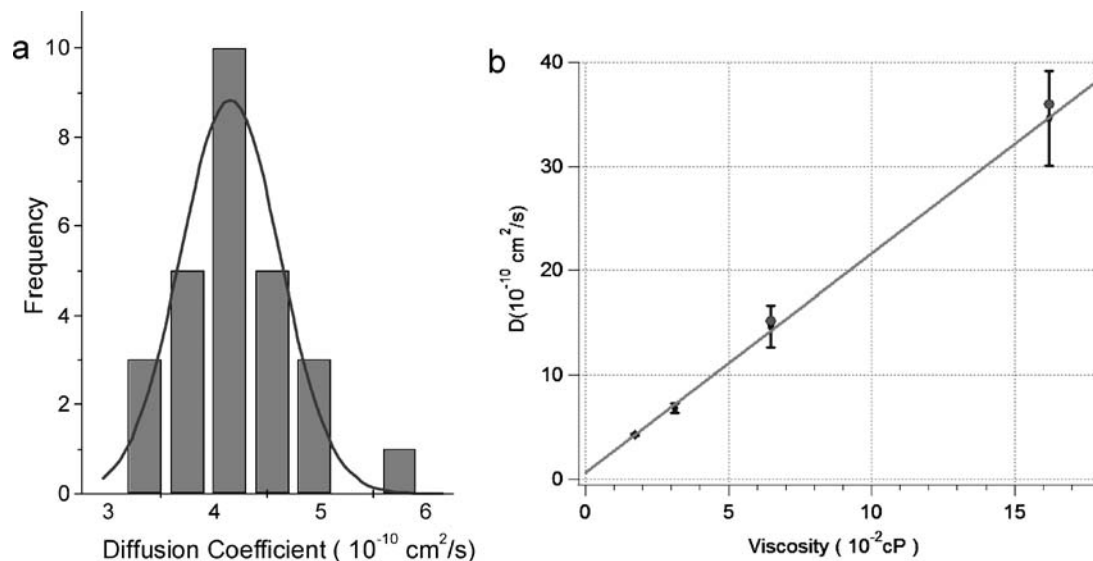
Fig. 5. (a) The distribution of diffusion coefficients for 10 trajectories of 200 nm particles tracked in 60% sucrose. The distribution is roughly Gaussian as expected and is centered about the theoretically expected diffusion coefficient predicted from the Stokes–Einstein relation. (b) Recovered diffusion coefficients for 60, 50, 56, and 40% sucrose solutions as a function of inverse viscosity. The graph shows the expected linear relationship and slope predicted by the Stokes–Einstein equation. Volumetric data: observation method (*black dots*), aberration method (*blue dots*).

paramagnetic particles using a magnetic trap. This approach has several attractive features. First, we are able to apply relatively high forces (nN) to the particle needed to produce substantial cellular strain. Additionally since the force is applied to a localized area on the cell, we can probe heterogeneities in the cell structure that would otherwise be concealed if we used other techniques that applied a force over relatively large area of the cell.

Figure 6a is a wide-field image of the cells plated on the coverslip. The cells have attached themselves to the coverslip and are spread out over the coverslip surface. The outlines of the cells are clearly visible as are the magnetic particles, which appear as large dark circles in the image. In Fig. 6, there is one magnetic sphere in the lower left-hand corner of the image. It is attached to the cell as are several polystyrene spheres, which are dimmer in the wide-field image. The polystyrene spheres are clearly visible in a two-photon fluorescent image of the same region as is the outline of the magnetic particle, which allow us to accurately quantify the distance from the polystyrene spheres to the magnetic particle (Fig. 6b).

Figure 7a shows the 3D trajectory that we obtained when we applied a rectified sine wave of force 1 nN and frequency of 1.3 Hz to the magnetic bead on the cell shown in Fig. 6. Since we are using a single-pole trap, it is only possible to apply force in one direction. The geometry of the experimental setup is such that the major portion of the force is applied along the x axis in the negative direc-

tion with only negligible force along the positive z-axis. Nevertheless, as is shown by Fig. 7a, the major portion of the motion that we observed was in the axial direction. The axial motion had an amplitude of approximately 400 nm, and the x-axis had an amplitude of 100 nm. The y-axis, on the other hand showed little motion beyond what was expected for noise. This plot clearly shows that for magnetic bead microrheometry experiments, appreciable 3D motion exists for forcing the motion to lie on a single plane. Aberration tracking method was used in all the experiments that we performed on the cells.

The force on the cell was increased to 2 nN by moving the magnetic pole closer to the cell which would produce larger deflections of the bead. Figure 7b is the trajectory of the same sphere as tracked in Fig. 7a. The sudden force applied to the cell when the trap was turned on at $t = 2$ s is evident as is the beginning of the recovery process when the trap was turned off at $t = 27$ s. The z-motion is approximately the same but the x-motion has increased as has the y-motion. Additionally, the motions in all three traces are in phase with one another at the frequency of the trap at 1.3 Hz. A long term creep response was also observed but was not investigated. Long-term responses may also be affected by active cellular processes such as cytoskeletal remodeling.

Figure 7c demonstrates the response of a cell to a toggled force. The cell displayed classic viscoelastic behavior that has been observed by other researchers. We
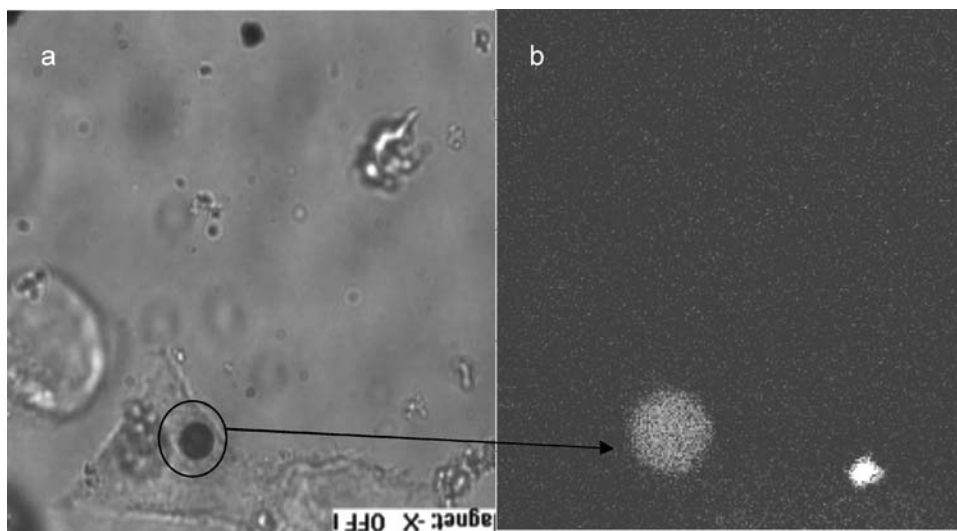
Fig. 6. (a) Wide-field image of the 293 embryonic kidney cells. The magnetic bead is clearly visible near the lower *left corner* of the image. (b) A two-photon fluorescent image of the same reason where the magnetic particle and the bright 500 nm latex sphere can be seen.

observed a three-phasic response similar to what Bausch (1998) observed, consisting of an initial elastic deflection, followed by a relaxation and then a flow response.

The creep experiments allow us to make estimates of the stiffness of the cell by analyzing the elastic portion of the response curve. The stress–strain relationship for a material is given by

$$\sigma = Y\varepsilon \qquad (9)$$

where σ is the stress (the force divided by the area the force is applied over) and ε is the strain (the ratio of the deflection by the unstretched length). This can be rewritten as

$$Y = \frac{FL_0}{\pi R^2 \Delta L} \qquad (10)$$

where F is the applied force, L_0 the effective unstretched length of the portion of the cell under tension, R the effective radius of the magnetic sphere in contact with the cell, and ΔL the deflection the cell undergoes due to the force.

We can make rough estimates for these parameters. From Fig. 1, the force on the particle is roughly 2 nN. We estimate the radius of the portion of the magnetic bead in contact with the cell to be of the order of 2 μm. The elastic portion of the creep response (in Fig. 7c) gives deflection (ΔL). The entire magnitude of the deflection is not used because we are only interested in the elastic response of the cell, and not in any fluid viscous behavior that predominates in the latter part of the deflection curve

[17]. For the un-stretched length, we have to estimate the spatial extent of the force applied to the cell at a point. Bausch *et al*. [17] and others have shown that there is a decay field around the magnetic particle and after a certain distance the effects of pulling on the sphere are no longer observed. We observed that if a polystyrene bead was more than 10–15 μm away from the magnetic sphere we would not see a deflection of the polystyrene sphere, for force level up to tens of nanonewton exerted on the magnetic bead. Therefore, we use an estimate of 15 μm for the L_0. This is in agreement with what others have observed. Substituting these values into Eq. (10) gives us a value of the order of 10^4 Pa for the Young's modulus, which is in the middle range of what other experimenters have observed for this parameter.

DISCUSSION

Instrumentation

The aim of the present work is to construct a particle tracking system based on the two-photon microscope that can track particles in all the three dimensions, at a high frequency response, and over an extended axial range, and to use this instrument to investigate an inherently 3D biological systems. We were able demonstrate the ability of the instrument to track particles in three dimensions. Both the volumetric method and the aberration method are straightforward to implement. There are trade offs in the two techniques. The aberration method is faster and
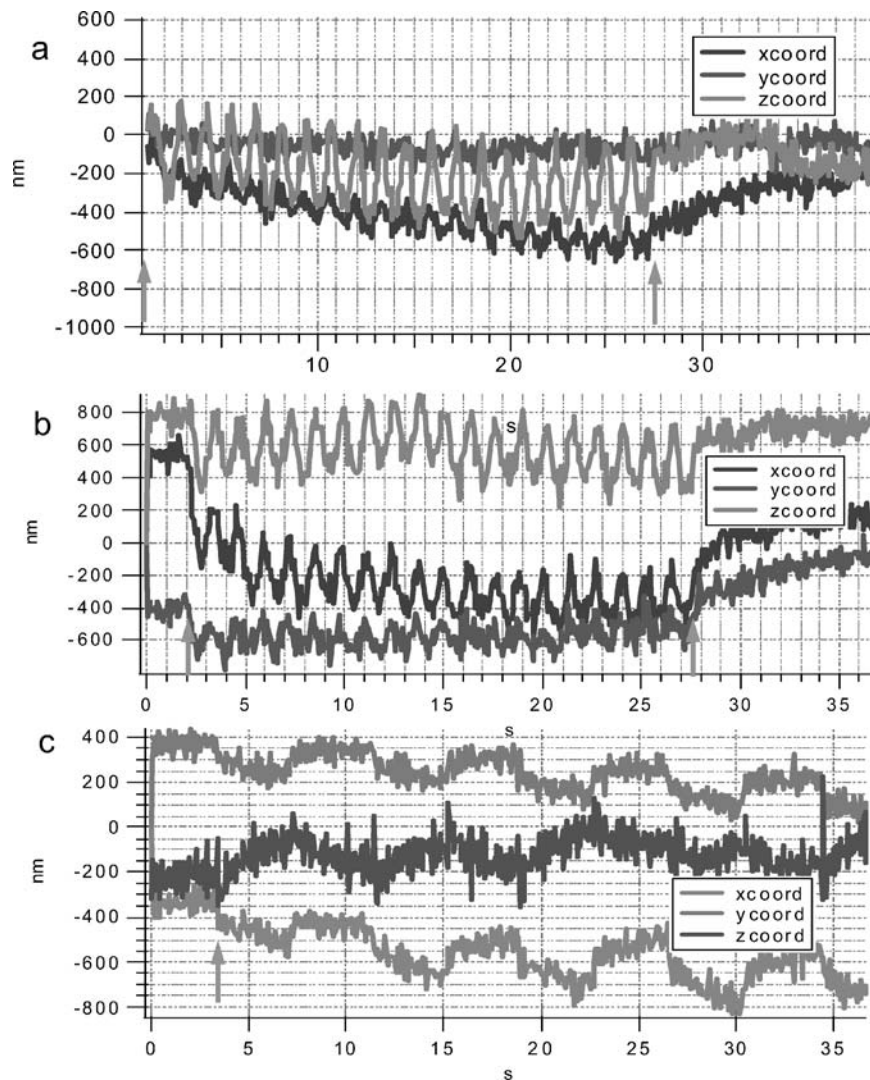
Fig. 7. (a) The 3D trajectory of a 500 nm sphere attached to the surface of the cell as the cell experiences an oscillatory force of 1 nN and 1.3 Hz from a magnetic bead attached to the surface approximately 7–8 μm away. The major portion of the motion is in the axial direction even though the major component of the force is along the negative x-direction. While all three axes display oscillatory motion, the x-axis experiences a gradual creep in the direction of the trap. When the trap is turned off at time 28 s there is a recovery in the position to the initial value for all three axes. (b) The motion of the bead shown in Fig. 7a as an oscillatory force of 2 nN and 1.3 Hz is applied to the cell beginning at time 2 s and ending at time 27 s. The larger force leads to larger deflections; however, the response is nonisotropic in the axes and nonlinear in magnitude with respect to the relative forces. The axes are offset from the origin at time 0 for clarity. (c) The magnetic trap was toggled on and off at periodic intervals with a force of 2 nN and the creep response of the cell was observed. The *arrows* indicate where the trap was toggled on and off.

generally more accurate. This arises mainly from the fact that it is only necessary to scan a single plane in order to acquire the full 3D position of the particle. It is not necessary to reposition the objective multiple times just to determine the coordinates of the particle. This repositioning takes time and potentially introduces artifacts arising from vibrations due to the mechanical contact between the objective lens, the immersion oil, and the coverslip. In general, the aberration method is the preferred technique, and that is why we opted for it in the cell mechanics studies. However, the volumetric tracking method does have some advantages. First, by scanning the full 3D volume

we are acquiring more information, which may be useful in some applications. For example, if we were interested in tracking two closely spaced particles, the volumetric method may be the only way, to do this as the aberration method depends on analyzing the shape of the images. If the two point spread functions of the particles overlap in the *x–y* plane, it will be difficult to do this. Secondly, since there are no aberrations in the optical system in the volumetric tracking method, the images will be brighter than they are in the aberration method, which has a larger and more diffuse PSF.

Cell Mechanics

As discussed previously, magnetic bead microrheometry has several attractive features. Well-controlled forces in the range of nanometer can be exerted on the cell, which can produce deformation from tens of nanometers to a few micrometers, and it is possible to quantify these motions at a high temporal and spatial resolution. Additionally, these forces can be applied to localized portions of the cell, which allows the spatial heterogeneity of the cell to be probed. Overall, magnetic bead microrheometry is a powerful technique for acquiring detailed kinetics and dynamics of the mechanical response of cells to extracellular forces. An aspect that previous magnetic bead microrheometry studies lacked was the ability to quantify the response in all three dimensions. Studies have shown that the three dimensional behavior of cells is an important element of the overall behavior [15,19,20]. To fully understand the mechanical properties of cells and the biological implications of those properties it will be necessary to study the full 3D motion of cells and not just a 2D projection of the motion of cells in response to stress.

Huang *et al*. demonstrated nonisotropic 3D deformation of the cytoskeleton framework by applying planar forces at the surface of the cell using magnetic bead microrheometry [15]. They were able to directly observe the effect these forces have on the 3D internal structure of the cell by visualizing the actin framework within the cell with an actin-GFP expression system, and observed that a planar stress applied at the surface of the cell altered the overall 3D structure of the cell in an nonisotropic manner, including the nuclear membrane structure. Deformations of the nuclear membranes are particularly interesting as they can directly alter the transcription of various genes through the modification of the 3D chromatin organization.

Helmke *et al*. investigated hemodynamic stress on endothelial cells by employing cells expressing GFP-vimentin system [19,20]. This study also emphasized the importance of studying the 3D behavior of the cellular response to stress. They observed that flow-induced displacement of the endothelial cells was greater near the apical surface of the cells, but did not decay as a simple function of depth from the apical surface, indicating that the displacement depended on the cytoskeletal morphology and was not a simple shear displacement. Additionally, 3D motion was often observed that would not have been visible in 2D projections of the same movement.

We also observed 3D motion of the cell in response to planar stresses. Significant motion was observed in all three dimensions even though the applied stress was primarily parallel to the coverslip surface. Moreover the stress response was complex and a greater stress did not affect the strain response in all three dimensions equally. This reinforces the anisotropic nature of cellular motion and the importance of studying the full 3D motion of the cell. 2D projections of the images we acquired would have significantly underestimated the amount of strain experienced by the cell and not captured the complex 3D dynamics of the system.

The present work provided accurate measurements of the strain response in the axial direction. This type of information will help clarify the exact mechanism by which extracellular forces are transmitted into the cytoplasm. This will be important in clarifying the role extracellular forces have on altering the nuclear architecture and consequently gene expression, the transmission of lateral hemodynamic stress in the lumenal wall throughout the arterial tree, as well as providing insight into the mechanical properties of the 3D cytoskeletal framework.

CONCLUSIONS

We have constructed a novel SPT instrument-based two-photon microscope that simultaneously tracks particles in all three dimensions using two different but related techniques. The volumetric scanning approach has a frequency response of approximately 6 Hz and is very straightforward to implement. The aberration method allows us to track the particles in all the three dimensions at a current maximum rate of 28 Hz. We tested the instrument by moving the sample in well-defined trajectories with an XY piezo scanner attached to the microscope and tracking diffusing particles with both the techniques. The data we have obtained so far are all self-consistent and establish the fact that the basic methodology we have developed is sound.

Additionally, the mechanical response of the cells to applied forces was studied. We observed significant *z*-motion of the cell that is important for the proper modeling of the cytoskeletal structure and dynamics. It is not possible to observe this sort of behavior when using

techniques that only look at a 2D projection of the motion. These experiments prove the usefulness of following the 3D motion of this system.

The technique can be improved in a number of relatively easy ways. First, the galvanometer scanner we are using is an older model and its bandwidth is limited to 500 Hz. Current scanners can go as fast as 2 kHz, which will gives us a factor of four increase in performance, and allow us to track particles with a frequency response over 100 Hz. Second, we can incorporate simultaneous DIC infrared wide-field imaging, which will allow us to monitor the position of the particle relative to any larger structures of interest. This would be of particular interest where the global structure of the sample is also changing, such as in cell migration experiments, or in cell mechanics studies. A fourth avenue we are pursuing is the incorporation of a multifoci scanning system into the two-photon microscope. This will allow us to scan over a larger volume (a 100 μm $\times$ 100 μm $\times$ 10 μm slab) and thus track multiple particles at once over a whole cell and establish mechanotransductive force decay fields of cells in 3D.

ACKNOWLEDGMENTS

REFERENCES

1. L. S. Barak and W. W. Webb (1981). Fluorescent low-density lipoprotein for observation of dynamics of individual receptor complexes on cultured human-fibroblasts. *J. Cell Biol.* **90**(3), 595–604.
2. M. Debrander, G. Geuens, R. Nuydens, M. Moeremans, and J. Demey (1985). Probing microtubule-dependent intracellular motility with nanometer particle video ultramicroscopy (nanovid ultramicroscopy). *Cytobios.* **43**(174), 273–283.
3. T. Fujiwara, K. Ritchie, H. Murakoshi, K. Jacobson, and A. Kusumi (2002). Phospholipids undergo hop diffusion in compartmentalized cell membrane. *J. Cell Biol.* **157**(6), 1071–1081.
4. K. Murase, T. Fujiwara, Y. Umemura, K. Suzuki, R. Iino, H. Yamashita, M. Saito, H. Murakoshi, K. Ritchie, and A. Kusumi (2004). Ultrafine membrane compartments for molecular diffusion as revealed by single molecule techniques. *Biophys. J.* **86**(6), 4075–4093.
5. K. Kis-Petikova and E. Gratton (2004). Distance measurement by circular scanning of the excitation beam in the two-photon microscope. *Microsc. Res. Tech.* **63**(1), 34–49.
6. A. Yildiz, J. N. Forkey, S. A. McKinney, T. Ha, Y. E. Goldman, and P. R. Selvin (2003). Myosin V walks hand-over-hand: Single fluorophore imaging with 1.5-nm localization. *Science* **300**(5628), 2061–2065.
7. H. Bornfleth, P. Edelmann, D. Zink, T. Cremer, and C. Cremer (1999). Quantitative motion analysis of subchromosomal foci in living cells using four-dimensional microscopy. *Biophys. J.* **77**(5), 2871–2886.
8. D. D. Li, J. Xiong, A. L. Qu, and T. Xu (2004). Three-dimensional tracking of single secretory granules in live PC12 cells. *Biophys. J.* **87**(3), 1991–2001.
9. W. F. Marshall, A. Straight, J. F. Marko, J. Swedlow, A. Dernburg, A. Belmont, A. W. Murray, D. A. Agard, and J. W. Sedat (1997). Interphase chromosomes undergo constrained diffusional motion in living cells. *Curr. Biol.* **7**(12), 930–939.
10. D. Thomann, D. R. Rines, P. K. Sorger, and G. Danuser (2002). Automatic fluorescent tag detection in 3D with super-resolution: Application to the analysis of chromosome movement. *J. Microsc. Oxf.* **208**, 49–64.
11. R. M. Dickson, D. J. Norris, Y. L. Tzeng, and W. E. Moerner (1996). Three-dimensional imaging of single molecules solvated in pores of poly(acrylamide) gels. *Science* **274**(5289), 966–969.
12. I. M. Peters, Y. van Kooyk, S. J. van Vliet, B. G. de Grooth, C. G. Figdor, and J. Greve (1999). 3D single-particle tracking and optical trap measurements on adhesion proteins. *Cytometry* **36**(3), 189–194.
13. M. Speidel, A. Jonas, and E. L. Florin (2003). Three-dimensional tracking of fluorescent nanoparticles with subnanometer precision by use of off-focus imaging. *Opt. Lett.* **28**(2), 69–71.
14. H. P. Kao, A. S. Verkman. (1994). Tracking of Single Fluorescent Particles in 3 Dimensions - Use of Cylindrical Optics to Encode Particle Position. *Biophys. J.* **67**(3), 1291–1300.
15. H. Huang, C. Y. Dong, H.-S. Kwon, J. D. Sutin, R. D. Kamm, and P. T. C. So (2002). Three-dimensional cellular deformation analysis with a two-photon magnetic manipulator workstation. *Biophys. J.* **82**(4), 2211–2223.
16. A. R. Bausch, W. Moller, and E. Sackmann (1999). Measurement of local viscoelasticity and forces in living cells by magnetic tweezers. *Biophys. J.* **76**(1 Pt 1), 573–579.
17. A. Bausch, F. Ziemann, A. Boulbitch, K. Jacobson, and E. Sackmann (1998). Local measurements of viscoelastic parameters of adherent cell surfaces by magnetic bead microrheometry. *Biophys. J.* **75**, 2038–2049.
18. H. Huang, R. D. Kamm, PTC So, and R. T. Lee (2001). Receptor-based differences in human aortic smooth muscle cell membrane stiffness. *Hypertension* **38**(5), 1158–1161.
19. B. P. Helmke, A. B. Rosen, and P. F. Davies (2003). Mapping mechanical strain of an endogenous cytoskeletal network in living endothelial cells. *Biophys. J.* **84**(4), 2691–2699.
20. B. P. Helmke, D. B. Thakker, R. D. Goldman, and P. F. Davies (2001). Spatiotemporal analysis of flow-induced intermediate filament displacement in living endothelial cells. *Biophys. J.* **80**(1), 184–194.